CHAPTER ONE

INTRODUCTION

The areas of machine tools, metal cutting, computer numerically controlled (CNC), computer-aided manufacturing (CAM), and sensor-assisted machining are quite wide, and each requires the academic and engineering experience to appreciate a manufacturing operation that uses all of them in an integrated fashion.

Although it is impossible to be an expert in all these subjects, a manufacturing engineer must be familiar with the engineering fundamentals for the precision and economical manufacturing of a part. This book emphasizes only the fundamentals of metal cutting mechanics, machine tool vibrations, feed drive design and control, CNC design principles, sensor-assisted machining, and the technology of programming CNC machines. The book is based on more than 120 journal articles and more than 60 research theses that reflect the engineering, research, and teaching experience of the author.

The book is organized as follows.

Chapter Two covers the fundamentals of metal cutting mechanics. The mechanics of two-dimensional orthogonal cutting is introduced first. The laws of fundamental chip formation and friction between the rake and flank faces of a tool during cutting are explained. The relationships among the workpiece material properties, tool geometry, and cutting conditions are presented. Identification of the shear angle, the average friction coefficient between the tool's rake face and moving chip, and the yield shear stress during machining is explained. The oblique geometry of practical cutting tools used in machining is introduced. The mechanics of oblique cutting for three-dimensional practical tools are explained, and methods in predicting the cutting forces in all directions are presented with the use of the laws of oblique cutting mechanics. The mechanics of turning, milling, and drilling, which constitute the majority of machining operations in the manufacturing industry, are presented. Algorithms for predicting the milling forces in three Cartesian coordinates are derived and illustrated with sample experimental results. Efficient force prediction algorithms for widely used helical end mills are presented. The chapter also briefly discusses the modes and causes of tool wear and breakage, that are important in evaluating the machinability of parts.

Chapter Three deals with static deformations and vibrations during machining. The static deformations occur because of the elastic deflections of both parts and machine during machining. When the static deformation is beyond the tolerance limit, the part is scrapped. Sample formulations are provided to predict the magnitude and location of static deformations in bar turning and end milling. The methods can be extrapolated to other machining operations such as grinding and drilling. One of the most common problems in machining originates from dynamic deformations (i.e., relative structural vibrations between the tool and workpiece). The most common vibrations are due to self-excited chatter vibrations, which grow until the tool jumps out of the cutting zone or breaks because of the exponentially growing dynamic displacements between the tool and workpiece. To understand the machine tool vibrations, the fundamental principles of single – and multi–degree-of-freedom vibration theory are summarized first. Because the machine tool chatter is mainly investigated by analyzing experimental data, the fundamentals of the experimental modal analysis techniques are presented. The modal analysis technique allows the engineer to represent a complex machine tool or workpiece structure by a set of commonly used mathematical expressions that engineers can understand. The technique not only allows one to analyze the chatter vibrations, but it gives a clear message to the machine tool engineer about the structural source of the vibrations during machining, which leads to the improved design.

Chapter Four presents the theory of chatter vibrations in both orthogonal and oblique machining operations both in the frequency and discrete time domain. The mathematical model of regenerative vibrations, which occur in subsequent tool passes during machining, is presented. The methods of determining chatter vibration–free axial depths of cuts and spindle speeds in orthogonal cutting operations are presented with and without process damping. Mathematical models of predicting chatter stability in turning, drilling, and milling operations are introduced. The techniques are explained with the aid of results obtained from simulation and machining tests. The engineer is presented with methods that increase the machining productivity by avoiding chatter vibrations.

Chapter Five introduces the CNC technology and its principles of operation and programming. First, standard NC commands accepted by all CNC machine tools are summarized. These include the format of an NC code accepted by the CNC of the machine tool, motion commands such as linear and circular contouring along a tool path, miscellaneous commands such as spindle and coolant control, and automatic cycles. Later, the introductory principles of CAM are presented. NC programs generated by CAM systems are processed by CNC units that generate position commands to each drive based on trajectory generation and real-time interpolation algorithms. The mathematical details of generating smooth trajectory with velocity, acceleration, and jerk limits of the machine are covered. Real-time interpolation of linear, circular, and splined paths are presented with examples.

Engineers who know how to use and program CNC machine tools must familiarize themselves with the design and internal operational principles of CNC. Chapter Six describes the fundamentals of CNC design, starting with the selection of drive motors and servoamplifiers. Mathematical modeling of feed servodrives is presented in detail. The transfer functions of mechanical drive inertia and friction, servomotor, amplifier, and velocity and position feedback sensors are explained with their practical interpretations. The transformation of continuous-time domain models of the physical system into discrete computer time domain models is explained. Design and tuning procedures for the digital control of feed drives are presented with real-life examples. Advanced control techniques for precision tracking and active vibration damping of feed drives are presented. The chapter is complemented with the design of electrohydraulic machine tool drives to show that the CNC design principles are general and can be applied to any mechanical system regardless of the actuators.

The recent trend in machining is to add intelligence to the machine tools and CNC, as discussed in Chapter Seven. Sensors that can measure the forces, vibrations, temperature, and sound during machining are installed on the machine tools. Mathematical models that correlate the relationship between the measured sensor signals and the state of machining are formed. The mathematical models are coded into real-time algorithms that monitor the machining process and send commands to CNC for corrective actions. The chapter includes simple but fundamental machining process control algorithms along with their theoretical foundations. Adaptive control of cutting forces, in-process monitoring of tool failure, and chatter detection algorithms are presented with their experimental validation and engineering application.

Sample problem sets are included at the end of each chapter. The problems mostly originated from the actual design, application, and experiments conducted at the author's manufacturing automation research laboratory; hence, they are designed to give a realistic feeling for engineering students. Because the book contains multiple engineering disciplines applied to machine tool engineering problems in an integrated fashion, most of the basic mechanical engineering concepts are assumed to be understood by the readers. However, the basic principles of Laplace and z transforms, as well as least squares – based identification techniques, are provided in the appendix.

The advanced mathematical models developed in the author's laboratory are simplified to teach the basic principles of metal cutting mechanics, machine tool vibrations, and control in this second edition of the book. The details of the full mathematical models are published in the research theses of graduate students and journal articles supervised by the author. The advanced algorithms are also packaged in CUTPRO © Advanced Machining Process Simulation Software [66], which is licensed to research centers and machining industry worldwide.

CHAPTER TWO

MECHANICS OF METAL CUTTING

2.1 INTRODUCTION

The final shapes of most mechanical parts are obtained by machining operations. Bulk deformation processes, such as forging and rolling, and casting processes are mostly followed by a series of metal-removing operations to achieve parts with desired shapes, dimensions, and surface finish quality. The machining operations can be classified under two major categories: cutting and grinding processes. The cutting operations are used to remove material from the blank. The subsequent grinding operations provide a good surface finish and precision dimensions to the part. The most common cutting operations are *turning*, *milling*, and *drilling* followed by special operations such as *boring, broaching, hobing, shaping*, and *form cutting*. However, all metal cutting operations share the same principles of mechanics, but their geometry and kinematics may differ from each other. The mechanics of cutting and the specific analysis for a variety of machining operations and tool geometries are not widely covered in this text. Instead, a brief introduction to the fundamentals of cutting mechanics and a comprehensive discussion of the mechanics of milling operations are presented. Readers are referred to established metal cutting texts authored by Armarego and Brown [25], Shaw [96], and Oxley [83] for detailed treatment of the machining processes.

2.2 MECHANICS OF ORTHOGONAL CUTTING

Although the most common cutting operations are three-dimensional and geometrically complex, the simple case of two-dimensional orthogonal cutting is used to explain the general mechanics of metal removal. In orthogonal cutting, the material is removed by a cutting edge that is perpendicular to the direction of relative tool–workpiece motion. The mechanics of more complex three-dimensional oblique cutting operations are usually evaluated by geometrical and kinematic transformation models applied to the orthogonal cutting process. Schematic representations of orthogonal and oblique cutting processes are shown in Figure 2.1. The orthogonal cutting resembles a shaping process with a straight tool whose cutting edge is perpendicular to the cutting velocity (V). A metal chip with a width of cut (b) and depth of cut (h) is sheared away from the workpiece. In orthogonal cutting, the cutting is assumed to be uniform along the cutting edge; therefore, it is a two-dimensional plane strain deformation process without side spreading of the material. Hence, the cutting forces are exerted only in the directions of velocity and uncut chip thickness, which are called tangential (F_t) and feed forces (F_f). However, in oblique cutting, the cutting edge is oriented with an inclination angle (i) and the additional third force acts in the radial direction (F_r).

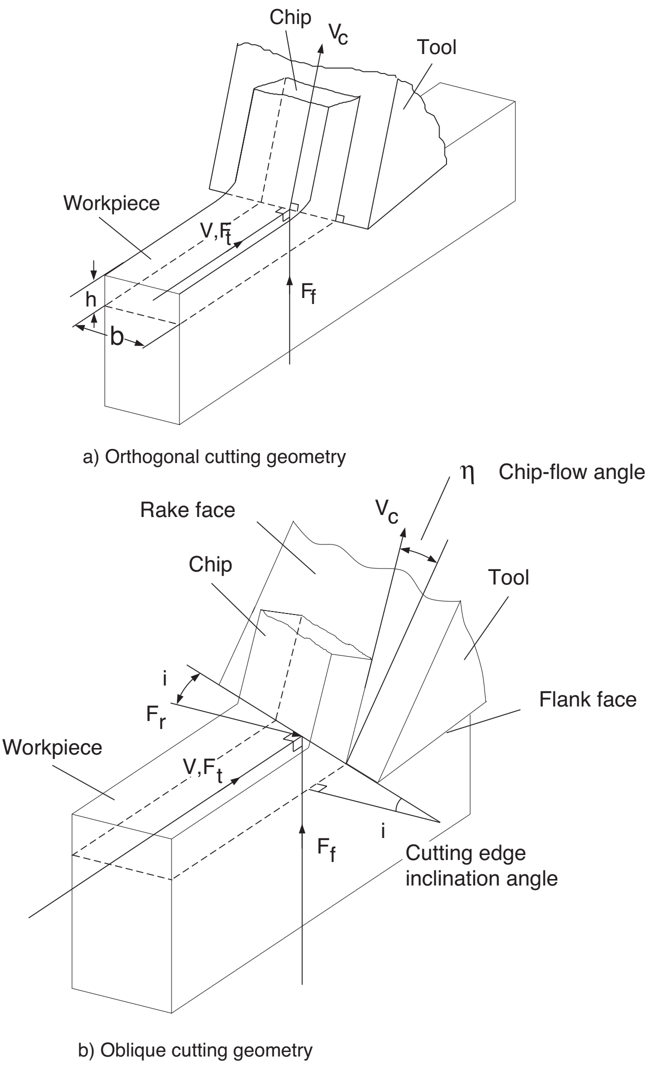

Figure 2.1: Geometries of orthogonal and oblique cutting processes.

There are three deformation zones in the cutting process as shown in the cross-sectional view of the orthogonal cutting (see Fig. 2.2). As the edge of the tool penetrates into the workpiece, the material ahead of the tool is sheared over the primary shear zone to form a chip. The sheared material, the chip, partially deforms and moves along the rake face of the tool, which is called the secondary deformation zone. The friction area, where the flank of the tool rubs the newly machined surface, is called the tertiary zone. The chip initially sticks to the rake face of the tool, which is called the *sticking region*. The friction stress is approximately equal to the yield shear stress of the material at the sticking zone where the chip moves over a material stuck on the rake face of the tool. The chip stops sticking and starts sliding over the rake face with a constant *sliding friction* coefficient. The chip leaves the tool, losing contact with the rake face of the tool. The length of the contact zone depends on the cutting speed, tool geometry, and material properties. There are basically two types of assumptions in the analysis of the primary shear zone. Merchant [75] developed an orthogonal cutting model by assuming that the shear zone is a thin plane. Others, such as Lee and Shaffer [67] and Palmer and Oxley [84], based their analysis on a thick shear deformation zone, proposing "shear angle

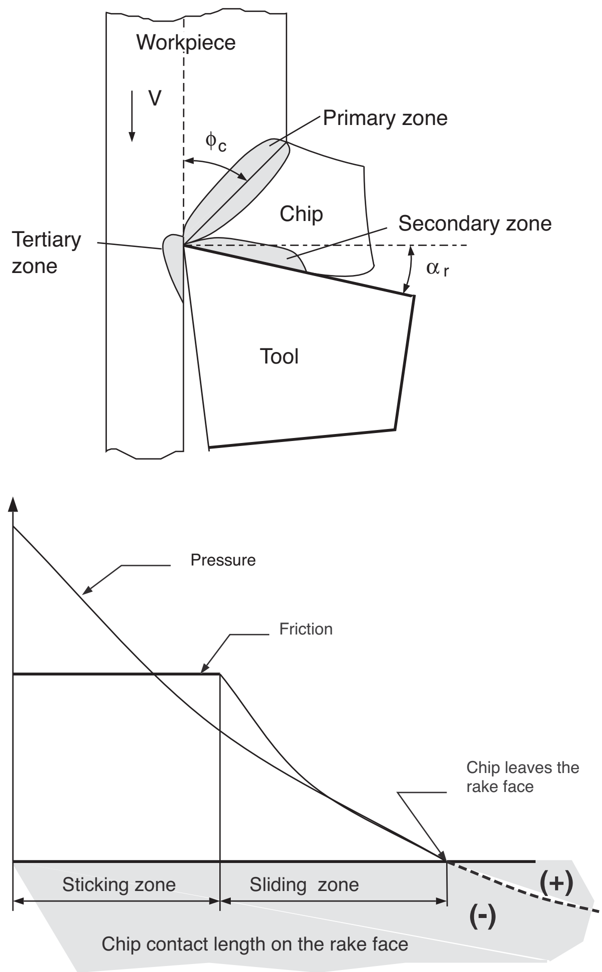

Figure 2.2: Contact zone (−) and tensile stresses (+) after the chip

prediction" models in accordance with the laws of plasticity. In this text, the primary shear deformation zone is assumed to be a thin zone for simplification.

The deformation geometry and the cutting forces are shown on the cross-sectional view of the orthogonal cutting process (see Fig. 2.3). It is assumed that the cutting edge is sharp without a chamfer or radius and that the deformation takes place at the infinitely thin shear plane. The shear angle ϕ_c is defined as the angle between the direction of the cutting speed (V) and the shear plane. It is further assumed that the shear stress (τ_s) and the normal stress (σ_s) on the shear plane are constant; the resultant force (F_c) on the chip, applied at the shear plane, is in equilibrium to the force (F_c) applied to the tool over the chip–tool contact zone on the rake face; an average constant friction is assumed over the chip–rake face contact zone. The contact forces originating from tertiary zone are assumed to be zero, and all cutting forces are due to shearing process or chip–rake face contact. From the force equilibrium, the resultant force (F_c) is formed from the feed (F_{fc}) and tangential (F_{tc}) cutting forces:

$$F_c = \sqrt{F_{tc}^2 + F_{fc}^2}. \tag{2.1}$$

The feed force (or thrust force) is in the direction of uncut chip thickness, and the tangential cutting force (or power force) is in the direction of cutting velocity. The cutting forces acting on the tool will have equal amplitude but opposite directions with respect to the forces acting on the chip. The mechanics of orthogonal cutting for two deformation zones are shown as follows.

Primary Shear Zone

The shear force (F_s) acting on the shear plane is derived from the geometry as follows:

$$F_s = F_c \cos(\phi_c + \beta_a - \alpha_r), \tag{2.2}$$

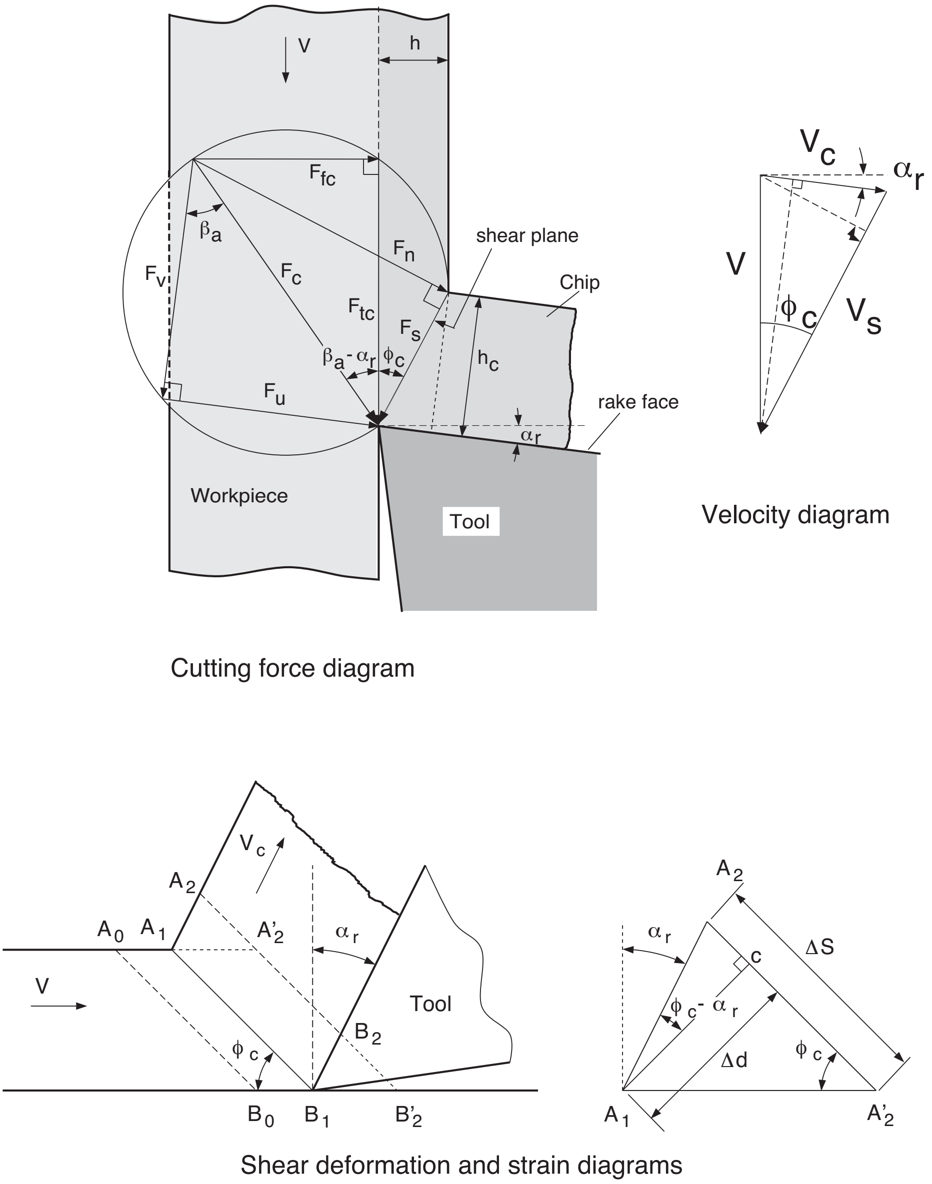

Figure 2.3: Mechanics of orthogonal cutting.

where β_a is the average friction angle between the tool's rake face and the moving chip, and α_r is the rake angle of the tool. The shear force can also be expressed as a function of the feed and tangential cutting forces as follows:

$$F_s = F_{tc} \cos \phi_c - F_{fc} \sin \phi_c. \tag{2.3}$$

Similarly, the normal force acting on the shear plane is found to be

$$F_n = F_c \sin(\phi_c + \beta_a - \alpha_r) \tag{2.4}$$

or

$$F_n = F_{tc} \sin \phi_c + F_{fc} \cos \phi_c. \tag{2.5}$$

With the assumption of uniform stress distribution on the shear plane, the shear stress (τ_s) is found to be

$$\tau_s = \frac{F_s}{A_s}, \tag{2.6}$$

where the shear plane area (A_s) is

$$A_s = b \frac{h}{\sin \phi_c}, \tag{2.7}$$

where b is the width of cut (or the depth of cut in turning), h is the uncut chip thickness, and (ϕ_c) is the shear angle between the direction of cutting speed (V) and the shear plane. The normal stress on the shear plane (σ_s) is

$$\sigma_s = \frac{F_n}{A_s}. \tag{2.8}$$

The cutting velocity (V) is resolved into two components (see the velocity diagram shown in Fig. 2.3). The material is sheared away from the workpiece with the shear velocity (V_s). From the velocity hodograph shown, we have

$$V_s = V \frac{\cos \alpha_r}{\cos(\phi_c - \alpha_r)}. \tag{2.9}$$

The shear power spent in the shear plane is

$$P_s = F_s \cdot V_s, \tag{2.10}$$

which is converted into heat. The corresponding temperature rise on the shear plane (T_s) is

$$P_s = m_c c_s (T_s - T_r), \tag{2.11}$$

where m_c is the metal removal rate [kg/s], c_s is the specific coefficient of heat for the workpiece material [Nm/kg$^\circ$C], and T_r is the shop temperature. The metal removal rate is found from the cutting process conditions,

$$\left.\begin{aligned} m_c &= Q_c \rho, \\ Q_c &= bhV \quad [\mathrm{m}^3/\mathrm{s}], \end{aligned}\right\} \tag{2.12}$$

where ρ[kg/m^3] is the specific density of the workpiece material. The shear plane temperature (T_s) can be calculated from Eqs. (2.9) to (2.12):

$$T_s = T_r + \frac{P_s}{m_c c_s}. \tag{2.13}$$

The formulation given above considers that the entire plastic deformation takes place only at the shear plane and that all the heat is also consumed at the shear plane. This assumption is shown to overestimate the temperature prediction proposed by Boothroyd [30], who considered that some of the plastic deformation takes place over a shear zone of finite thickness and that some of the heat is dissipated to the work material and the chip, away from the thin shear plane. Oxley [83] used the following modified temperature prediction:

$$T_s = T_r + \lambda_h(1-\lambda_s)\frac{P_s}{m_c c_s}, \tag{2.14}$$

where λ_h ($0 < \lambda_h \leq 1$) is a factor that considers the plastic work done outside the thin shear zone, and λ_s is the proportion of the heat conducted into the work material. For a plain carbon steel, an average value for $\lambda_h \approx 0.7$ can be assumed [107]. The heat conducted into the work material is evaluated with the following experimentally evaluated empirical equation [83]:

$$\begin{aligned} \lambda_s &= 0.5 - 0.35\log(R_T \tan\phi_c), \quad \text{for} \quad 0.04 \leq R_T \tan\phi_c \leq 10, \\ \lambda_s &= 0.3 - 0.15\log(R_T \tan\phi_c), \quad \text{for} \quad R_T \tan\phi_c \geq 10, \end{aligned} \tag{2.15}$$

where ϕ_c is the shear angle and R_T is a nondimensional thermal number given by

$$R_T = \frac{\rho c_s V h}{c_t}, \tag{2.16}$$

where c_t is the thermal conductivity of the work material with units [W/(m°C)]. Note also that the heat transmitted to the work material can not be more than the total energy generated, and a negative influx of the heat into the shear plane is not possible ($0 \leq \lambda_s \leq 1$).

The shear plane length L_c is found from the chip deformation geometry as follows:

$$L_c = \frac{h}{\sin\phi_c} = \frac{h_c}{\cos(\phi_c - \alpha_r)}. \tag{2.17}$$

The chip compression ratio (r_c) is the ratio of the uncut chip thickness over the deformed (h_c) one as follows:

$$r_c = \frac{h}{h_c}. \tag{2.18}$$

The shear angle is found from the geometry as a function of rake angle and the chip compression ratio as follows:

$$\phi_c = \tan^{-1}\frac{r_c\cos\alpha_r}{1 - r_c\sin\alpha_r}. \tag{2.19}$$

The shear strains and strain rates in metal cutting are significantly higher than those found from standard tensile tests and metal-forming operations. The geometry of a deformed chip is shown in Figure 2.3. Assume that an undeformed chip section $A_0B_0A_1B_1$ is moving with workpiece velocity V. The workpiece material is deformed plastically at the shear plane (B_1A_1), and the cut chip slides over the rake face with a chip velocity V_c. After Δt shearing time, the uncut metal strip $A_0B_0B_1A_1$ becomes a chip with a geometry of $A_1B_1B_2A_2$. Hence, the chip is shifted from the expected position $B_2'A_2'$ to the deformed position B_2A_2 because of shearing in the shear plane with a shear angle of

ϕ_c. Because of plane strain deformation, $A_2'A_2 = B_2'B_2$. The shear strain (γ_s) is defined as the ratio of deformation ($\Delta s = A_2'A_2$) over the nominal distance between the deformed and undeformed planes ($\Delta d = A_1C$) as follows:

$$\gamma_s = \frac{\Delta s}{\Delta d} = \frac{\overline{A_2A_2'}}{\overline{A_1C}} = \frac{\overline{A_2'C}}{\overline{A_1C}} + \frac{\overline{CA_2}}{\overline{A_1C}} = \cot\phi_c + \tan(\phi_c - \alpha_r).$$

By rearranging, the shear strain can be expressed as

$$\gamma_s = \frac{\cos\alpha_r}{\sin\phi_c\cos(\phi_c - \alpha_r)}. \tag{2.20}$$

The shear strain rate is

$$\gamma_s' = \frac{\gamma_s}{\Delta t}.$$

Assuming that the shear zone increment is Δs and that the thickness of shear deformation zone is Δd, the shear strain and shear velocity can be defined as $\gamma_s = \Delta s/\Delta d$ and $V_s = \Delta s/\Delta t$, respectively. The shear strain rate is then defined as

$$\gamma_s' = \frac{V_s}{\Delta d} = \frac{V\cos\alpha_r}{\Delta d\cos(\phi_c - \alpha_r)}. \tag{2.21}$$

Because the shear zone thickness Δd is extremely small in cutting, Eq. (2.21) indicates the presence of very high shear strain rates. Especially when the shear zone is assumed to be a plane with zero thickness, the strain rate becomes infinite, which can not be true. However, the thin shear plane approximation is useful for the macromechanics analysis of metal cutting. For practical and approximate predictions, the thickness of the shear zone can be approximated as a fraction of the shear plane length (i.e., $\Delta d \approx 0.15$–$0.2\,L_c$). For more accurate analysis, the shear zone thickness must be evaluated by freezing the machining process with a quick stop test and measuring the zone thickness with a scanning electron microscope (SEM).

Secondary Shear Zone

Two components of the cutting force are acting on the rake face of the tool (Fig. 2.3): the normal force F_v,

$$F_v = F_{tc}\cos\alpha_r - F_{fc}\sin\alpha_r, \tag{2.22}$$

and the friction force F_u on the rake face,

$$F_u = F_{tc}\sin\alpha_r + F_{fc}\cos\alpha_r. \tag{2.23}$$

In the orthogonal cutting analysis shown here, it is assumed that the chip is sliding on the tool with an average and constant friction coefficient of μ_a. In reality, the chip sticks to the rake face for a short period and then slides over the rake face with a constant friction coefficient [119]. The average friction